Abdominal Radiology

© Springer Science+Business Media New York 2016
Published online: 2 January 2017

Abdom Radiol (2017) 42:742–748
DOI: 10.1007/s00261-016-1023-1

Metal implants on CT: comparison of iterative reconstruction algorithms for reduction of metal artifacts with single energy and spectral CT scanning in a phantom model

Jieming Fang, Da Zhang, Carol Wilcox, Benedikt Heidinger, Vassilios Raptopoulos, Alexander Brook, Olga R. Brook

Department of Radiology, Beth Israel Deaconess Medical Center, Rosenberg Building, Office 378, One Deaconess Drive, 330 Brookline Avenue, Boston, MA 02215, USA

Abstract

Purpose: To assess single energy metal artifact reduction (SEMAR) and spectral energy metal artifact reduction (MARS) algorithms in reducing artifacts generated by different metal implants.

Materials and method: Phantom was scanned with and without SEMAR (Aquilion One, Toshiba) and MARS (Discovery CT750 HD, GE), with various metal implants. Images were evaluated objectively by measuring standard deviation in regions of interests and subjectively by two independent reviewers grading on a scale of 0 (no artifact) to 4 (severe artifact). Reviewers also graded new artifacts introduced by metal artifact reduction algorithms.

Results: SEMAR and MARS significantly decreased variability of the density measurement adjacent to the metal implant, with median SD (standard deviation of density measurement) of 52.1 HU without SEMAR, vs. 12.3 HU with SEMAR, $p < 0.001$. Median SD without MARS of 63.1 HU decreased to 25.9 HU with MARS, $p < 0.001$. Median SD with SEMAR is significantly lower than median SD with MARS ($p = 0.0011$). SEMAR improved subjective image quality with reduction in overall artifacts grading from 3.2 ± 0.7 to 1.4 ± 0.9, $p < 0.001$. Improvement of overall image quality by MARS has not reached statistical significance (3.2 ± 0.6 to 2.6 ± 0.8, $p = 0.088$). There was a significant introduction of artifacts introduced by metal artifact reduction algorithm for MARS with 2.4 ± 1.0, but minimal with SEMAR 0.4 ± 0.7, $p < 0.001$.

Conclusion: CT iterative reconstruction algorithms with single and spectral energy are both effective in reduction of metal artifacts. Single energy-based algorithm provides better overall image quality than spectral CT-based algorithm. Spectral metal artifact reduction algorithm introduces mild to moderate artifacts in the far field.

Key words: Iterative reconstruction—Metal artifact reduction—Dual energy—Single energy—Phantom comparison—Computed tomography

Metal implants can cause substantial artifacts on CT imaging due to the attenuation of X-rays as they pass through metallic substances [1], which is detrimental for diagnostic image quality. Numerous methods have been applied to reduce the metal artifacts with none producing results with artifact-free image. A recent innovation using iterative reconstruction methods has shown to reduce the severity of metallic artifacts. Iterative reconstruction and metal artifact reduction (MAR) can be performed with either single energy or spectral (dual energy) techniques. Previous research has shown spectral MAR to be partially effective in the case of hip prostheses [2], gold fiducials in the abdomen [3], and iodine-125 seeds in the liver [4], whereas single energy MAR has proven effective for vascular occlusion coils in the abdomen [1, 6], dental implants [5], and hip prostheses [6].

To date, there has only been one comparison study [7] about the relative efficacies of these two artifact reduction techniques for prosthetic hip implants. Our goal was to evaluate two iterative reconstruction algorithms that use single energy MAR vs. spectral MAR with a wider

Correspondence to: Olga R. Brook; *email:* obrook@bidmc.harvard.edu

variety of metallic vascular implants for the ability to reduce metal artifacts and improve overall image quality in a controlled environment of a phantom model.

Materials and methods

A CT phantom was constructed in-house with three different densities (water, saline solution, and ultrasound gel) and placed atop a commercial CT head calibration phantom (Mindways Software, Austin, TX, USA). The phantom container was approximately 17 cm by 17 cm, and filled with water to a depth of 4 cm (Figure 1). The phantom was scanned with the following parameters: 120 kVp, CTDIvol = 21 mGy, SFOV = 40 cm, DFOV = 19.3 cm, with single energy (0.5 s tube rotation, 380 mAs tube current, 3 mm slice thickness, axial scanning mode) and spectral imaging (0.6 s tube rotation, 640 mAs tube current, 2.5 mm slice thickness, helical scanning mode) to serve as a base for comparison for underlying densities. Parameters were set first on the dual energy scanner, and then settings were adjusted on the single energy scanner to match CTDIvol on the dual energy scanner. A metal implant was then inserted into the phantom and the phantom was scanned with single energy and spectral CT scanners with and without MAR algorithms applied. The process was repeated for each type of metal implant: Amplatzer vascular plug 4 (St. Jude Medical, St. Paul, Minnesota, USA), 15 mm embolization coil (Penumbra, Alameda, California, USA), 8 × 40 mm expandable stent (Wallstent Endoprosthesis, Boston Scientific, Boston, Massachusetts, USA), 6 × 40 mm biliary stent (E-Luminexx, Bard Peripheral Vascular, Tempe, Arizona, USA), gold fiducial seed (Censis Technologies, Franklin, Tennessee, USA).

Fig. 1. In-house constructed phantom, consistenting of 17 cm × 17 cm plastic container with water, a saline solution filled bag, and ultrasound gel. This is placed on top of a commercial CT head calibration phantom (Mindways, Austin, TX USA).

Single energy CT with single energy metal artifact reduction (SEMAR) was performed with a 320 multidetector CT scanner (Aquilion One, Toshiba Medical Systems, Otawara, Japan) and images with and without SEMAR were reconstructed on a Vitrea Workstation (Toshiba Medical Systems, Otawara Japan). Spectral CT with metal artifact reduction software (MARS) was performed with 64 multidetector CT scanner (Discovery CT750 HD, General Electric Healthcare, Milwaukee, Wisconsin, USA). Reconstructions were made with 30% statistical iterative reconstruction. A dedicated workstation (GE Advantage Workstation 4.5, GE Healthcare) was used to reconstruct images at 77 keV without MARS and 77 keV with MARS. The 77 keV level reconstruction level was chosen to be equivalent to 120 kVp and is standard for clinical abdominal CT angiography examinations at our institution, as higher keV levels would reduce the level of contrast enhancement. Scanners are calibrated daily to ensure Hounsfield Unit accuracy of 0 ± 3 HU for the spectral energy scanner and 0 ± 5 HU for the single energy scanner according to vendor specifications. Images were evaluated on Centricity Picture Archiving and Communication System (GE Healthcare) with readers free to adjust window levels as they saw fit.

Both SEMAR and MARS use iterative reconstruction techniques to reduce metal artifacts. The artifact reduction process starts with segmenting out metallic artifacts in the forward projection data. Data from the areas surrounding the artifacts are used to interpolate corrected projection data which are used to replace the artifact data. The corrected data are further segmented to remove metallic traces then forward projected and reconstituted with the original data [1]. MARS also uses dual energy techniques by leveraging the ability of the Discovery CT750 scanner to switch between 80 and 140 keV every 0.25 ms during scan acquisition. Materials that show similar attenuations at one voltage may show different attenuations at another voltage, thus dual energy CT may be better able to distinguish features and materials including metals and metal-induced artifacts [7].

Objective evaluation

Three identical regions of interest (ROI) of minimum size of 1000 pixels were obtained: (1) from image with metal implant with worst artifact without MAR algorithm; (2) corresponding ROI at the same level and in-slice location with MAR algorithm applied; and (3) baseline images without metal implant and therefore without any artifacts and without application of MAR algorithms. One triplet set was obtained with single energy MAR and the other one with spectral MAR.

ROIs were obtained adjacent to different types of metal implants causing artifacts: Amplatzer plug ($n = 1$), embolization coil ($n = 2$), gold fiducials ($n = 7$), or stents ($n = 10$). This produced 20 triplet sets of ROIs, each for single energy and spectral MAR algorithms.

Mean standard deviations of HU across ROI were compared with the Mann–Whitney test with significant cut-off value set at $p < 0.05$. Histograms of select ROI were used to aid visual analysis of the data.

Subjective evaluation

Images featuring metal implants were evaluated with and without the application of single energy and spectral MAR. The images were presented randomly and blindly to the method that they were obtained (with or without metal artifact reduction algorithm, which type) to avoid bias. The images were independently evaluated by a fellowship-trained interventional and abdominal radiologist with 14 years of experience and a radiology research fellow with 1 year of imaging experience who had received specific training from the attending radiologist prior to evaluation. Each image was given an overall grade as well as sub-categorical grades based on artifact location (near or far field) and artifact type (bloom, shadow, and streak). In addition, images were evaluated and graded for additional artifacts introduced by the MAR algorithms.

All subjective grades were assigned a score of 0 (unimpaired readability and no artifact), 1 (artifact present but no significant impairment), 2 (mildly impaired readability), 3 (moderately impaired image readability), and 4 (severely impaired readability).

Interobserver agreement was assessed with kappa statistics. Statistical comparisons of grades within each paired set were made with t test (significance level $p < 0.05$).

Results

Objective evaluation

Our objective metric is focused on noise reduction within the ROI. Objective evaluation of spectral MAR and single energy MAR techniques showed significant differences in the standard deviation of density in ROI adjacent to the metal implant between images at the baseline, with and without artifact reduction. These differences are depicted on histograms of individual ROI which show the distribution of pixel count vs. pixel value (HU) for baseline, with reduction and without reduction (Figures 2, 3, 4). Baseline pixel distributions are tightly centered around the mean pixel value, resulting in a single narrow, peaked histogram shape. Pixel distributions without reduction are more scattered, resulting in wider, lower peaks. After artifact reduction, the shape of

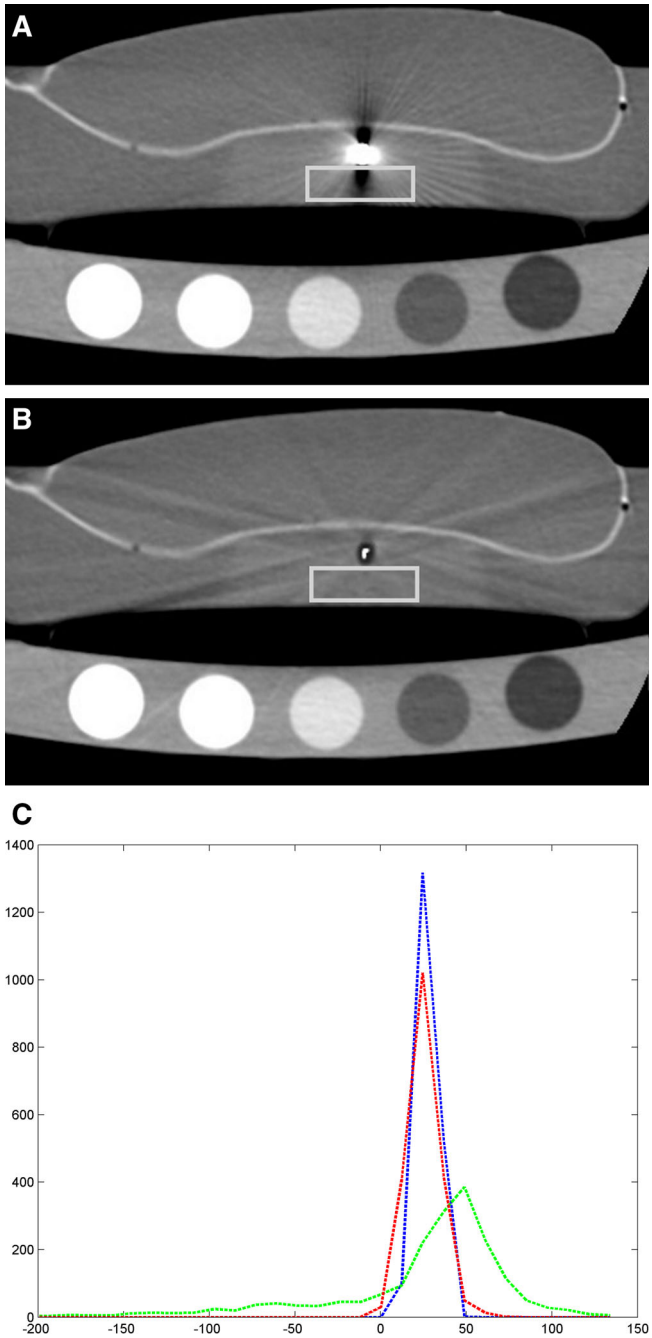

Fig. 2. **A** Spectral CT scan of fiducial seed embedded into ultrasound gel produces severe near-field shadow and bloom artifacts. Moderate to mild streak artifacts extend into the far fields. ROI used for objective measurement is marked by *white rectangle*. **B** Post-processing with spectral MAR effectively eliminates near-field bloom and reduces near-field shadow to a ring around the fiducial seed. Far-field streak artifacts are more prominent due to the introduction of new artifacts. **C** Histogram showing pixel count (*Y*-axis) vs. pixel HU (*X*-axis). Distribution curve within ROI without spectral MAR (*green*) has a lower, wider peak whereas distribution curve with spectral MAR (*red*) much more closely resembles baseline distribution curve (*blue*) in height, shape, and location.

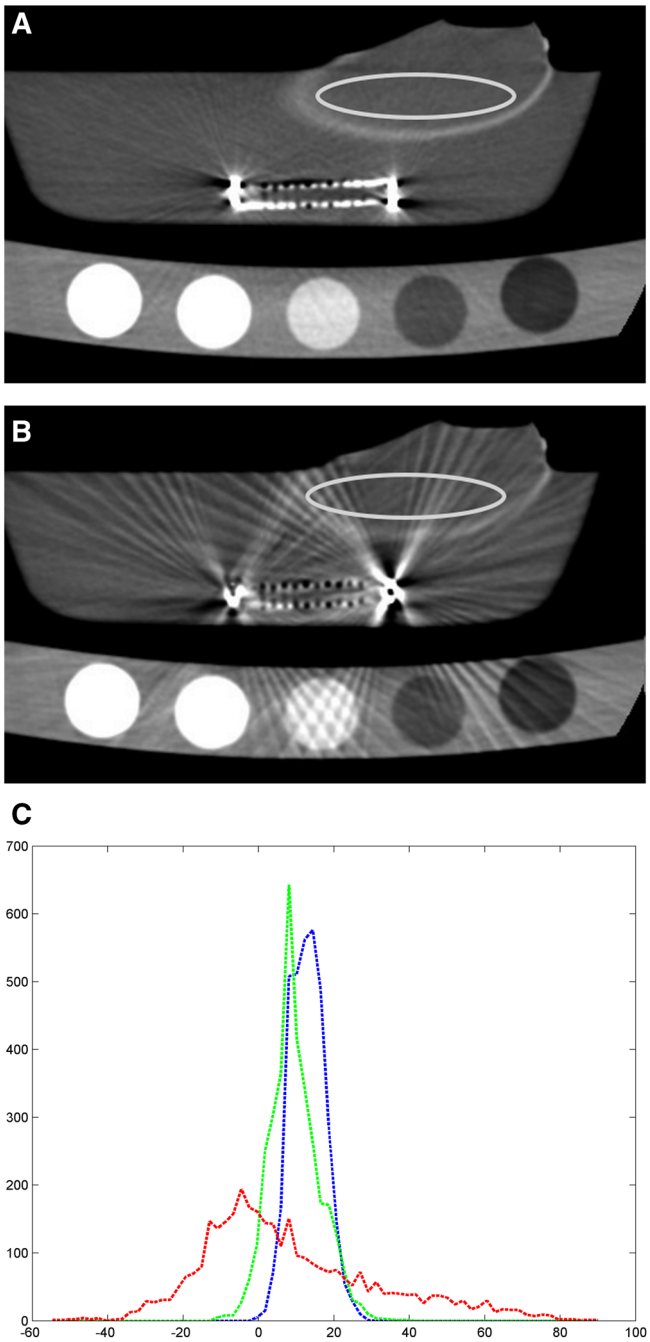

Fig. 3. **A** Spectral CT scan of stent placed in water with ROI (*white ellipse*) drawn in near-field saline solution. Bloom and shadow artifacts are most severe near either end of the stent, due to the placement of radiopaque markers. Mild streak artifacts are present in the ROI. **B** Post-processing with spectral MAR introduces a severe amount of streak artifacts originating from the ends of the stent and extending to the far field. New bloom and shadow artifact are also visible near the ends of the stent. **C** Histogram that shows distribution curve without spectral MAR (*green*) is very similar to baseline distribution curve (*blue*). Application of spectral MAR causes distribution curve (*red*) to be much more scattered and widely distributed without a singular peak due to the introduction of artifacts.

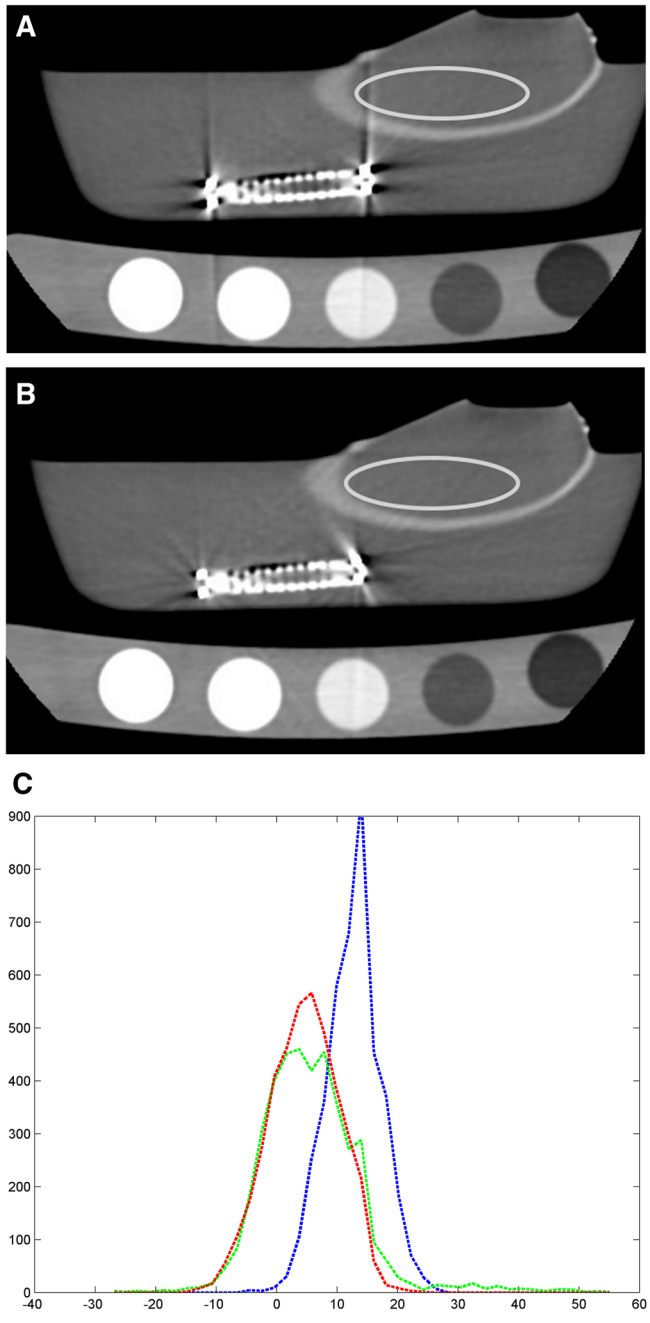

Fig. 4. **A** Single energy CT scan of stent placed in water with ROI (*white ellipse*) drawn in near-field saline solution. Bloom and shadow artifacts are most severe near either end of the stent, and dark streak artifacts extend vertically into the ROI and far-field areas. **B** Post-processing with single energy MAR effectively reduces near-field shadow and bloom artifacts and far-field streak artifacts. No additional artifacts are introduced in the image by the application of single energy MAR. **C** Histogram distribution curve for the ROI with single energy MAR (*red*) is slightly more peaked than without single energy MAR (*green*), therefore more closely resembling baseline (*blue*).

the distribution is more similar to baseline, with the exception of instances in which the reduction algorithm itself introduced new artifacts (Figure 3).

Application of spectral MAR reduced the standard deviation of the density measurement from 63.1 to 25.9 HU (Table 1). Single energy MAR brought standard deviations of density measurements from 52.1 to 12.3 HU for all metal implants collectively (Table 1).

Mann–Whitney–Wilcoxon test showed no significant differences ($p = 0.73$) in the standard deviations of uncorrected spectral energy images with implant (median 63.1 HU) vs. uncorrected single energy images with implant (median 52.1 HU), therefore the amount of noise is similar in uncorrected images with the two techniques. Standard deviation in the post-correction single energy MAR images (median 12.3 HU), however, was significantly lower ($p = 0.0011$) than that of the post-correction spectral MAR images (median 25.9 HU), therefore single energy MAR appears to be better for artifact reduction than spectral MAR.

Subjective evaluation

There was no significant subjective improvement in metal artifacts produced by spectral MAR in overall image quality, near-field bloom, near-field streak, far-field bloom, far-field shadow, and far-field streak. However, there was significant improvement in near-field shadow artifact with spectral MAR ($p = 0.03$) (Table 1).

Single energy MAR showed statistically significant improvements in overall image quality, near-field streak, near-field shadow, and no change in near-field bloom, far-field streak, far-field shadow, and far-field bloom (Table 1).

Spectral MAR also consistently introduced new artifacts (Table 2; Figure 3). In 10 out of 11 images (91%) with spectral MAR, streak artifacts in the near and far fields were introduced, each one with severity of grade 2 or above and one with severity of grade 4. Overall across all 11 images performed with spectral MAR, the average severity score of additional artifacts was 2.36 ± 1.03 (Table 2). In contrast (Figure 4), single energy MAR introduced additional artifact on 4 out of 12 images (33%), none with severity greater than grade 2, and with an overall grade for additional artifact across 12 images of 0.42 ± 0.67 (Table 2).

Interobserver agreement for subjective evaluation of the presence of artifacts had kappa value of 0.75. In the cases of disagreement between two readers, a consensus was reached following further discussion.

Discussion

Our study shows that both single energy and spectral MAR significantly reduce the standard deviation of HU in ROI with metal-induced artifacts. Standard deviations with single energy MAR were significantly lower than standard deviations with spectral MAR, suggesting that artifacts are more effectively reduced in severity by single

Table 1. For objective evaluation, standard deviation measurements (HU) were taken from identical regions of interest of at least 1000 pixels in size adjacent to the metal implant, without and with the application of MAR algorithms, and with comparison to the same area in the phantom scanned prior to incorporation of metal implants

Single energy MAR				Spectral MAR			
	Metal implant with MAR	Metal implant and no MAR	No metal implant		Metal implant with MAR	Metal implant and no MAR	No metal implant
Objective							
Stents ($n = 10$)	15.4	71.4	4.9	Stents	33.3	78.1	6.3
Fiducial seed ($n = 7$)	16.3	116.9	5.5	Fiducial seed	26.3	120.3	5.6
Amplatzer plug ($n = 1$)	5.8	6.2	5.1	Amplatzer plug	12.0	8.0	4.5
Embolization coil ($n = 2$)	13.5	78.9	4.8	Embolization coil	68.7	118.7	4.8

Single energy MAR				Spectral MAR			
	Metal implant with MAR	Metal implant and no MAR	*p* value		Metal implant with MAR	Metal implant and no MAR	*p* value
Subjective							
Near shadow	**1.8 ± 1.3**	**3.5 ± 1**	**0.0012**	Near shadow	**3 ± 1.4**	**4 ± 0**	**0.03**
Near bloom	0.83 ± 1.3	2.1 ± 1.8	0.065	Near bloom	0.82 ± 1.4	2.1 ± 1.9	0.091
Near streak	**1.5 ± 1**	**2.7 ± 1.4**	**0.031**	Near streak	3.1 ± 1.4	2.7 ± 1.4	0.55
Far shadow	0.25 ± 0.62	1.3 ± 1.7	0.063	Far shadow	0.55 ± 1.2	1.6 ± 2.0	0.13
Far bloom	0 ± 0	0.5 ± 1.2	0.15	Far bloom	0.36 ± 1.2	0.73 ± 1.6	0.56
Far streak	0.5 ± 0.67	1.3 ± 1.3	0.088	Far streak	2.6 ± 1.2	2.3 ± 1.6	0.55
Overall	**1.4 ± 0.51**	**3.2 ± 0.72**	**<0.0001**	Overall	2.6 ± 0.81	3.2 ± 0.6	0.88

Listed values are median standard deviations of those particular regions of interest. Subjective evaluations of images with metal implants with and without the application of MAR algorithms were based on 0 (no artifact) to 4 (severe) grades by two independent readers. Listed values represent mean grade ± standard deviation. Student *t* test was used to determine significant differences in reader grades between with and without MAR, bold indicates statistical significance ($p < 0.05$)

Table 2. Types and grades of additional artifacts introduced by MAR algorithms

Single energy MAR			Spectral MAR		
Image pair	Grade	Type of artifact	Image pair	Grade	Type of artifact
1	0		1	2	Streaks in near and far fields
2	0		2	2	Streaks in near and far fields
3	0		3	2	Streaks in near and far fields
4	0		4	3	Streaks in near and far fields
5	2	Streaks in the far field	5	2	Streaks in near and far fields
6	1	Streaks in the far field	6	3	Streaks in near and far fields
7	0		7	3	Streaks in near and far fields
8	1	Bloom in near field	8	2	Streaks in near and far fields
9	0		9	0	
10	1	Streaks in the near field	10	3	Streaks in the far field
11	0		11	4	Streaks in near and far fields
12	0				
Average	0.42 ± 0.67		Average	2.36 ± 1.03	

Each image pair contains one uncorrected image with metal implant, and one corrected image with metal implant and MAR active. Readers evaluated the corrected image for the presence of additional artifact introduced by each MAR algorithm, graded the severity of the artifacts from 0 (no artifact) to 4 (severe artifact), and described the type and location of the artifacts

energy MAR. Single energy MAR was able to produce significantly improved subjective grades in the overall image quality compared to the unreduced image, whereas spectral MAR showed no significant improvement in the overall image quality. Spectral MAR also consistently introduced additional artifacts of mild to moderate severity.

We have confirmed that MAR algorithms with iterative reconstructions are effective, as seen by decrease in the standard deviation measurements adjacent to the metal artifacts after the application of MAR. This is in accordance with prior studies which show that single energy MAR [1, 5] and spectral MAR [3, 4] reduce the standard deviations of HU when applied to ROI afflicted by artifact. Single energy MAR produced significantly lower standard deviations than spectral MAR. Artifact ROI on images acquired on the single energy CT scanner vs. the spectral CT scanner by different manufacturers with their respective MAR algorithms off were not significantly different, making it less likely that hardware differences between the two scanners are a factor in the performance gap.

In the subjective evaluation there is some discordance between our findings and previously published research. In our evaluation, spectral MAR failed to produce statistically significant improvement in overall readability, which was not the case in other studies [2–4]. Additional artifacts caused by spectral MAR were also more common here than in previous studies [3]. This may be due to the difference in implants being evaluated, as these previous studies examined prosthetic hips [2], gold fiducial markers [3], and radio-iodide seeds [4] rather than stents and coils as we did in our study. This behavior of spectral MAR was not entirely unknown, as previous studies [3, 8] showed what was called the "dark star" far-field artifact when applying the algorithm to gold fiducials. As we have shown here, however, this phenomenon is not limited to gold fiducials and has appeared with nearly every type of metal implants we studied. This phenomenon appeared in 10 out of 11 total images of our study (Table 2). The additional artifacts were most severe with one stent, although a different type of stent in the same spatial orientation did not display additional artifacts at all. This could be due to the different metal densities of balloon expandable vs. self-expanding stents. Single energy MAR introduced relatively mild and less frequent additional artifacts (Table 2) when applied to the same implants.

An earlier study indicated that these additional artifacts could be endemic to artifact reduction algorithms which rely on replacing artifact-afflicted signal with interpolated data from surrounding areas [9, 10]. There are alternative techniques centered on artifact signal deletion rather than replacement [11–13], but these methods have the potential drawback of blurring and loss of resolution around the metal implant due to loss of data.

The limitations of our study stem from small sample size and a limited variety of spatial orientations, including the fact that we only evaluated images in the axial plane. Whereas prior research was done in vivo [1, 3, 5, 9, 11], we elected to use a phantom. This allowed us to select the type and orientation of metal implants thus creating an identical benchmark for comparison between single energy and spectral MAR, but this is not a perfect analog for clinical application in a live patient. Although we could quantify and qualify the severity and nature of artifacts before and after the application of MAR algorithms, we could not evaluate how these artifacts and MAR techniques would have affected diagnostic accuracy in live patients with actual pathologies. Additionally, our phantom is not anthropomorphic and is much more homogenous than the inside of a human body which may account for some of the discrepancies in

results. For example, it was hypothesized that the metal implant's proximity to bone may cause some of the additional artifact [3] but this was not something we could investigate with our current phantom. We did not evaluate the differences in artifact severity between different implants, either different types of stents, or stents vs. coils vs. fiducial seeds, as we were primarily focused on the differences between the two MAR algorithms.

In conclusion, iterative reconstruction algorithms are able to reduce the severity of metallic artifacts. Given our phantom and selection of metal implants, we found the performance of single energy MAR to be superior to that of spectral MAR. Although the spectral MAR algorithm still shows improvement, single energy MAR performed better than spectral MAR in our phantom study with relatively small sample size. Further investigation is warranted to determine if single energy MAR's apparent advantage holds true under clinical conditions with patients.

Compliance with ethical standards

Funding No funding was received for this study.

Conflicts of interest The authors declare that they have no conflict of interest.

Ethical approval This article does not contain any studies with human participants or animals performed by any of the authors. For this type of study formal consent is not required.

Informed consent Statement of informed consent was not applicable since the manuscript does not contain any patient data.

References

1. Sofue, K, Yoshikawa, T, Negi, N, et al. Abdominal CT with single-energy metal artifact reduction (SEMAR): initial experiences. Poster session presented at: European Congress of Radiology, 2014 March 6–10, Vienna, Austria
2. Morsbach F, Bickelhaupt S, Wanner GA, et al. (2013) Reduction of metal artifacts from hip prostheses on CT images of the pelvis: value of iterative reconstructions. Radiology 268(1):237–244
3. Brook OR, Gourtsoyianni S, Brook A, et al. (2012) Spectral CT with metal artifacts reduction software for improvement of tumor visibility in the vicinity of gold fiducial markers. Radiology 263(3):696–705
4. Yang Q, Peng S, Wu J, et al. (2015) Spectral CT with monochromatic imaging and metal artifacts reduction software for artifacts reduction of (125)I radioactive seeds in liver brachytherapy. Jpn J Radiol 33(11):694–705
5. Funama Y, Taguchi K, Utsunomiya D, et al. (2015) A newly-developed metal artifact reduction algorithm improves the visibility of oral cavity lesions on 320-MDCT volume scans. Phys Med 31(1):66–71
6. Sonoda A, Nitta N, Ushio N, et al. (2015) Evaluation of the quality of CT images acquired with the single energy metal artifact reduction (SEMAR) algorithm in patients with hip and dental prostheses and aneurysm embolization coils. Jpn J Radiol 33(11):710–716
7. Andersson KM, Nowik P, Persliden J, et al. (2015) Metal artefact reduction in CT imaging of hip prostheses—an evaluation of commercial techniques provided by four vendors. Br J Radiol 88(1052):20140473
8. Barrett JF, Keat N (2004) Artifacts in CT: recognition and avoidance. Radiographics 24(6):1679–1691
9. Yu L, Li H, Mueller J, et al. (2009) Metal artifact reduction from reformatted projections for hip prostheses in multislice helical computed tomography: techniques and initial clinical results. Investig Radiol 44(11):691–696
10. Watzke O, Kalender WA (2004) A pragmatic approach to metal artifact reduction in CT: merging of metal artifact reduced images. Eur Radiol 14(5):849–856
11. Boas FE, Fleischmann D (2011) Evaluation of two iterative techniques for reducing metal artifacts in computed tomography. Radiology 259(3):894–902
12. Meyer E, Raupach R, Lell M, et al. (2010) Normalized metal artifact reduction (NMAR) in computed tomography. Med Phys 37(10):5482–5493
13. Prell D, Kyriakou Y, Kachelrie M, et al. (2010) Reducing metal artifacts in computed tomography caused by hip endoprostheses using a physics-based approach. Investig Radiol 45(11):747–754